



Effect of SiC Content and Hot Compaction on the Microstructure, Thermal, Mechanical, and Tribological Characteristics of Aluminum Matrix Nanocomposites Produced via Powder Metallurgy

Received 6 May 2025; Revised 3 August 2025; Accepted 5 August 2025

A. El-Sayed M. Hassan ¹
Ahmed M. Elmashad ²
Mohamed N. El-Sheikh ³
Moustafa M. Mohammed⁴
Mohamed Abu-Okail ⁵
Osama M. Irfan ⁶
A.M.I. Abu-Oqail ⁷

Keywords

Aluminium matrix
composites, hot
compaction, thermal
conductivity, mechanical
properties, tribological
behaviour, SiC particles

Abstract: This study investigates the effect of silicon carbide (SiC) content and hot compaction temperature on the microstructural, mechanical, tribological, and physical properties of Al/SiC nanocomposites. Composites were synthesized via high-energy ball milling followed by hot compaction, with SiC contents of 2.5, 5, 7.5, and 10 wt.% and compaction temperatures of 500 °C, 550 °C, and 600 °C. SEM revealed uniform dispersion and minimal agglomeration of SiC particles, particularly in the 5 wt.% SiC sample, with improved particle-matrix interfacial bonding. The 5 wt.% SiC composite compacted at 600 °C achieved the highest relative density ($98.2 \pm 0.5\%$) and exhibited the most significant performance improvements: wear rate decreased by 70% (from 4.95 ± 0.12 to $1.49 \pm 0.08 \times 10^{-5}$ g/min), compressive strength increased by 95% (from 325.8 ± 10.4 to 635.8 ± 15.2 MPa), and hardness rose by 45% (from 98 ± 2 to 179 ± 4 HV), compared to unreinforced Al. While ductility showed a slight decrease ($\sim 8\%$), thermal stability remained within acceptable limits for engineering applications. The findings suggest that 5 wt.% SiC reinforcement and a compaction temperature of 600 °C offer an optimal balance of properties suitable for load-bearing components in automotive and aerospace industrial.

1. Introduction

The proliferation of advanced materials in contemporary engineering is driven by the necessity to achieve specialized and specific product requirements. These requirements are often unattainable using single materials, leading to a surge in research focused on composite materials with tailored properties [1]. Among these, aluminum matrix composites (AMCs) have garnered significant attention due to their advantageous characteristics, including low density and favourable physical and mechanical properties [2-3]. B₄C/Al composites were

¹ Assoc. professor, Dept. Production Technology., Beni-Suef University, Beni-Suef, Egypt. a_sayed_hassan@yahoo.com

² Assist. Lecturer, Dept. Production Technology., Beni-Suef University, Beni-Suef, Egypt. Ahmedelmashad91@yahoo.com

³ Professor, Dept. Production Technology., Beni-Suef University, Beni-Suef, Egypt. Elsheikh53@hotmail.com

⁴ Assist. professor, Dept. Production Technology., Beni-Suef University, Beni-Suef, Egypt. engmos_m2020@yahoo.com

⁵ Lecture, Dept. Production Technology., Beni-Suef University, Beni-Suef, Egypt. Mohamed.okail20@yahoo.com

⁶ Professor, Department of Mechanical Engineering., Qassim University, Saudi Arabia. o.ahmed@qu.edu.sa

⁷ Assoc. professor, Dept. Production Technology., Beni-Suef University, Beni-Suef, Egypt. ahmed.abuoqail@gmail.com

fabricated via friction stir processing, with the threaded pin profile yielding the most uniform particle distribution. This improved homogeneity led to enhanced hardness and wear resistance in the stir zone. [4] A primary motivation for employing AMCs in advanced engineering applications is to enhance their wear resistance. The incorporation of ceramic reinforcements, such as SiC into the Al matrix has been demonstrated to improve these critical properties [5-7]. The primary objective of reinforcing composite materials is to enhance their physical, mechanical, and tribological properties. Research has shown that the performance of various reinforcements particularly when optimizing particle size and weight fraction significantly improves the microstructure and mechanical behavior of composites [8–10]. Among these, SiC particles are extensively employed as a reinforcement due to their effectiveness and versatility, finding widespread use in industries such as aerospace, automotive, and sports equipment manufacturing [10, 14-16]. This is due to the exceptional high-temperature stability, high strength, hardness, wear resistance, and cost-efficiency of SiC. Incorporating SiC particles into an aluminium matrix results in composites exhibiting enhanced physical, mechanical, and tribological performance. [17-18]. Powder metallurgy is widely acknowledged as an effective and advantageous technique to produce metal matrix composites. [19]. Hot compaction offers advantages over cold compaction in producing composites with enhanced properties, as it eliminates the need for additional sintering steps by simultaneously compacting and consolidating the material under heat and pressure. [20]. Yu, H. et al. [21] Ye, Tengke et al. [22] investigated how interface microstructure and porosity affect the mechanical and thermal properties of Al/SiC composites with high SiC volume fractions, fabricated through spark plasma sintering. The study revealed that increasing SiC content and sintering temperature generally enhanced thermal conductivity and flexural strength. However, at a sintering temperature of 520 °C, these properties along with density and interfacial bonding-were negatively impacted. The research also explored the role of SiC particle size on the mechanical behaviour of aluminium matrix composites. El-Kady, O. and Fathy [23] investigated the influence of SiC particle size and reinforcement content on the physical and mechanical characteristics of Al-SiC composites. Jiang et al. [24] studied the improvement in mechanical properties of SiC-reinforced aluminium alloys fabricated using the squeeze casting technique. Iqbal, A. K. M. et al. [25] examined the influence of sintering temperature and compaction pressure on the mechanical behavior of Al/SiC composites. The study showed that increasing both parameters improves density and hardness, thereby enhancing the overall mechanical properties of the material. Abu-Oqail, A. M. I. et al. [26] investigated the effect of different SiC contents on the microstructure, mechanical properties, and wear behavior of aluminum matrix composites produced by hot compaction. They found that a 5 wt.% SiC addition resulted in a uniform distribution of microparticles, which significantly improved hardness, compressive strength, wear resistance, and relative density. Canakci, Aykut, and Temel Varol [27] investigated the impact of hot extrusion on Al/SiC composites fabricated via powder metallurgy, finding that enhanced interparticle bonding substantially improved mechanical performance. They also observed that adding titanium led to a reduction in thermal conductivity. Ünlü et al. [28] assessed the mechanical and tribological behavior of aluminum matrix composites reinforced with SiC using powder metallurgy. The results showed that the reinforced composites displayed significantly better

mechanical and wear resistance properties than the unreinforced aluminum matrix. Akbari, Mostafa, et al. [29] demonstrated that Al-Si alloy-based surface hybrid composites reinforced with Al_2O_3 and SiO_2 using friction stir processing exhibit enhanced wear resistance. The composition containing 20% Al_2O_3 and 80% SiO_2 delivered the best performance by effectively balancing increased hardness with improved lubrication properties. Singh, Jaswinder [30] investigated the fabrication and wear characteristics of Al-SiC composites produced via powder metallurgy. The incorporation of SiC particles was found to significantly enhance the hardness of the composite material. Karamış, M. et al. [31-34] reported that under dry sliding conditions, reinforced Al-SiC composites exhibited both adhesive and abrasive wear mechanisms, whereas unreinforced AA6061 predominantly experienced adhesive wear. Surface roughness increased notably after wear testing but was not significantly influenced by the number of RE (rotational extrusion) passes.

This study investigates an innovative fabrication approach combining high-energy ball milling process to produce aluminum-based composites with enhanced performance. The primary objective is to develop materials exhibiting high strength, increased hardness, and elevated thermal conductivity, suitable for advanced engineering applications. By employing the hot-pressing technique for Al/SiC nanocomposites, this research aims to improve the physical, mechanical, and tribological properties of the aluminum matrix. The influence of varying temperatures and different concentrations of SiC nanoparticles on microstructural evolution, relative density, thermal conductivity, wear rate, and coefficient of friction (COF) is systematically examined to elucidate the mechanisms responsible for the improved composite performance.

2. Experimental work

2.1 Materials preparation

In this study, the metal matrix used was (Al) powder, with an average particle size of ~40 nm and a purity of 99.8% (Dop Organic Kimya, Ankara, Turkey), as shown in Figs. 1(a) and 2(a). The reinforcing phase (SiC) had an average particle size of ~50 nm and a purity of 98% (M K Impex Corp., Canada), as depicted in Figs. 1(b) and 2(b).

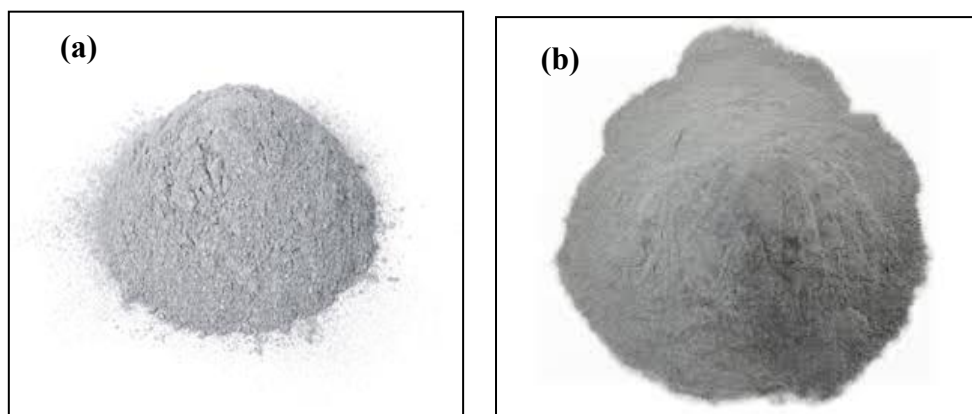


Fig.1: Raw materials before mixing process a) pure nano Al, b) nano-SiC

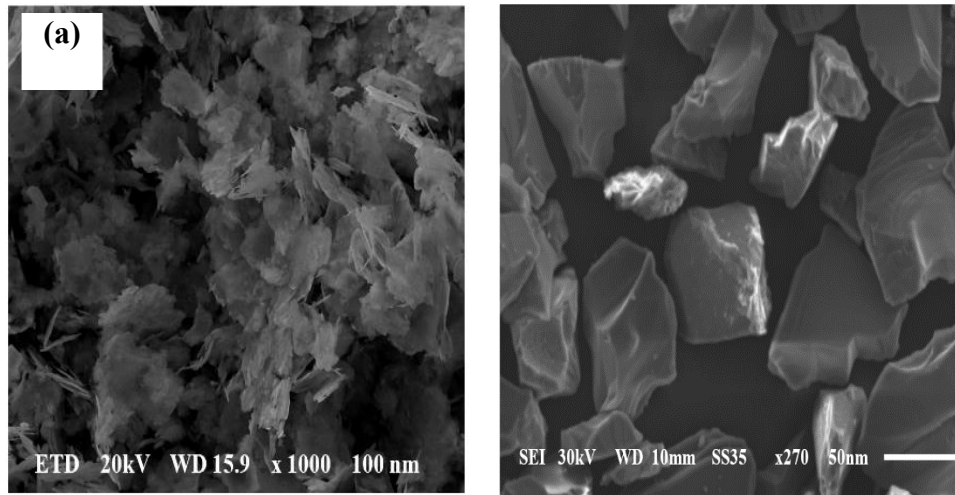


Fig. 2: FE-SEM of raw material before mixing process: a) pure nano Al, b) nano-SiC

To fabricate the Al/SiC nanocomposites powders the Al powder was mixed with different concentrations of SiC nanoparticles by high energy ball milling and different temperatures as shown in Table 1. To assess their effects on composite properties such as strength, physical characteristics, and wear resistance, while also ensuring uniform dispersion. The selected concentration ranges were chosen to prevent agglomeration at lower contents and optimize performance at higher contents.

Table 1. Experimental Process Parameters for Al/SiC Nanocomposites

Parameter	Description
Metal Matrix	Aluminum (Al) powder
Reinforcement	Silicon Carbide (SiC)
SiC Content (wt.%)	0, 2.5, 5, 7.5, 10
Milling Atmosphere	Dry air
Ball-to-Powder Ratio	16:1
Milling Media	Stainless steel balls (10 mm diameter)
Milling Duration	12 hr.
Rotational Speed	350 rpm
Compaction Method	Uniaxial hot compaction
Compaction Temperatures	500 °C, 550 °C and 600 °C
Compaction Pressure	900 MPa
Compaction Time	30 minutes
Loading speed	2 mm/min

At this stage, mechanical alloying was carried out using a ball milling process to ensure uniform blending and mixing of the powders. The milling of SiC was performed in a dry air atmosphere, while Al powders were milled under a protective argon (Ar) atmosphere to minimize oxidation. Stearic acid (1 wt.%) was used as a process control agent (PCA) to prevent excessive cold welding and to enhance powder flowability. The volume ratio of stainless-steel balls to the milling container was maintained at 3:1, with a ball-to-powder

weight ratio of 16:1, in accordance with the parameters reported in [35]. Each milling batch consisted of 25 g of powder, and 10 mm diameter stainless steel balls were used as the milling media. The milling was performed continuously at a rotational speed of 350 rpm for 12 hours, with periodic cooling intervals of 30 minutes every 3 hours to avoid overheating. The Al/SiC blended powders underwent uniaxial hot compaction at three distinct temperatures: 500 °C, 550 °C, and 600 °C. All specimens were pressed under a constant pressure of 900 MPa, with a loading speed of 2 mm/min and a holding time of processing time is 30 min.as shown in Fig.3.
















At Constant pressure = 900 Mpa										
Wt. % & a.den. Temp. ° c	0% SiC	Act. Density	2.5% SiC	Act. Density	5 % SiC	Act. Density	7.5 % SiC	Act. Density	10% SiC	Act. Density
500		2.7225		2.71861		2.76766		2.63767		2.5989
550		2.69708		2.65744		2.67327		2.65824		2.64749
600		2.819		2.7483		2.8824		2.6923		2.6658

Fig.3: Samples of hot compacted nanocomposite.

3. Testing characteristics

To investigate the microstructural features of the hot-compacted nanocomposites Al/SiC, the samples were metallographically prepared by polishing to a mirror-like finish using silicon carbide abrasive papers with grit sizes of 280, 600, 800, and 1000, followed by fine polishing on a cloth pad. Surface etching was then carried out using a standard etchant etch code 1000 to enhance contrast and reveal the substructural morphology. The etched samples were then examined using Field Emission Scanning Electron Microscopy (FE-SEM) FEI Quanta FEG 250) at 15 kV accelerating voltage, 8 mm working distance, and high vacuum mode with a secondary electron detector. Samples were sputter-coated with 5 nm Au to mitigate charging. Energy Dispersive X-ray Spectroscopy (EDAX) was utilized to characterize the elemental composition of the sample surfaces at 20 kV, 5 nA beam current, and 90 s live time calibrated against pure Al and SiC standards.

Phase analysis of hot-compacted samples was performed using X-ray diffraction (XRD) with a Bruker D8 Kristalloflex diffractometer employing Ni-filtered Cu K α radiation ($\lambda = 1.5406$ Å). The XRD patterns were collected over a 2θ range 10° - 90° to ensure detection of all phases

with a step size of 0.02 for resolution and a scan rate of 1-2 s/step. This technique was used to identify all crystalline phases present, detect any new phases formed, and determine the atomic arrangement within the composites. [36] The crystallite size (D) was estimated to be using the Scherrer equation [1]:

$$\Gamma = \frac{K \lambda}{\beta \cos \theta} \quad \text{Eq. (1)}$$

Where: Γ : Volume-weighted average crystallite size (in nm or Å).

K: Scherrer constant (dimensionless, ~0.89–0.94; typically, 0.9 for spherical crystallites).

λ : X-ray wavelength (e.g., Cu-K α = 1.5406 Å), β : Full width at half maximum (FWHM) of the diffraction peak after correcting for instrumental broadening (in radians).

θ : Bragg angle (in radians).

The relative density of the fabricated composites was determined using the Archimedes principle with water as the immersion medium, in accordance with the procedure outlined in [37]. Thermal conductivity was evaluated according to the ASTM E1004 standard. Measurements were conducted using a PCE-COM20 device, which was calibrated against the International Annealed Copper Standard (IACS) [38]. The thermal conductivity of the composites was calculated using the following equation [2]: -

$$K = \sigma \cdot L \cdot T \quad \text{Eq. (2)}$$

Where: K: thermal conductivity. (W/m.K), σ : Electrical conductivity. ($\Omega^{-1} \cdot \text{m}^{-1}$)

L: Lorentz number = $2.45 \cdot 10^{-8}$ (W. $\Omega \cdot \text{K}^{-2}$), T: kelvin temperature (K)

The manufactured composites were assessed using a Vickers microhardness tester (model number 1600-4981) according to ASTM E92-17 [39]. with a load application rate of 500 gf and dwell 15 sec. Prior to testing, the composites were polished using Grit sequence procedure. Microhardness measurements were conducted using two methods: (i) at specific points from center to circumference and (ii) along the circumference, to evaluate the impact of nanoparticle distribution on microhardness. For the circumference measurement, each sample was divided into three concentric circles radii (1.7, 3.3) mm with indentations placed at 45° increments. Measurements were taken on origin and two circles, resulting in seventeen-point indentations per sample, as shown in Fig.4 The microhardness values were obtained using a load of 0.5 kg_f and an indentation dwell time of 15 seconds. Vickers' hardness was calculated using the following equation [3]:

$$Hv = 1.8544 \cdot \frac{P}{d^2} \quad \text{Eq. (3).}$$

Compression testing was carried out using a computer-controlled servo-hydraulic universal testing machine (Model UH-500 kNA, Shimadzu, Version 2023, Japan), in accordance with ASTM E9 and ASTM E209 standards. Wear behaviour of Al/SiC nanocomposites were evaluated using the pin-on-disc technique in accordance with ASTM G99-17. The counter face consisted of a steel disc with a track diameter of 153 mm and an average surface roughness of 70 μm . Tests were conducted under dry sliding conditions at room temperature, with a constant sliding distance for all samples. The test specimens were circular pins with a diameter of 10 mm, yielding a contact area of 78.53 mm². while was applied the normal load 15 N. The sliding velocity was maintained at 1.2 m/s with a rotational speed of 150 RPM. The wear rate was calculated using the following equation [4] [40].

$$W = \frac{\Delta M}{L} \quad \text{Eq. (4)}$$

Where W is the wear rate (g /m), ΔM is change between the weight before and weight after of composite. L is the sliding distance of composite. The coefficient of friction COF for the tested composites sliding against a steel surface with roughness was determined by measuring both the frictional force and the applied normal force.

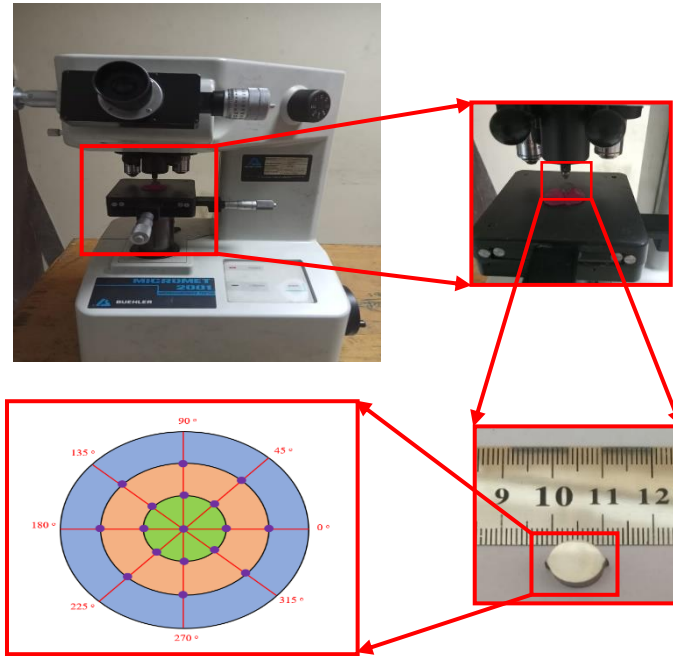


Fig.4: Vickers microhardness equipment and procedures.

4. Results and discussions

4.1 Microstructure, Mechanical and tribological properties of Al/SiC nanocomposites

Fig. 6 illustrates the influence of high-energy ball milling on the particle morphology and dispersion characteristics of Al/SiC composites with varying SiC content. The unreinforced Al matrix (Fig. 6a) exhibits a flake-like morphology with a narrow particle size distribution ($\sim 40 \pm 5$ nm), indicative of uniform plastic deformation during milling [41]. In the composite containing 2.5 wt.% SiC (Fig. 6b), a similar flake morphology is observed, accompanied by a homogeneous distribution of the reinforcement phase after 12 h of milling [42]. At 5 wt.% SiC (Fig. 6c), the microstructure evolves into elongated aggregate forms with a uniform dispersion of SiC particles within the Al matrix, reflecting enhanced interfacial bonding and mixing efficiency [43]. The 7.5 wt.% SiC composition (Fig. 6d) reveals irregularly shaped flakes, pronounced asymmetry, and an increase in average particle size, which can be attributed to the mismatch in deformation behavior between ductile Al and brittle SiC [44]. This mismatch impacts the composite's response to mechanical loading during milling, influencing particle overlaps, bonding behavior, and dispersion homogeneity. The composite with 10 wt.% SiC (Fig. 6e) exhibits significant agglomeration of elongated SiC clusters and reduced dispersion uniformity, likely due to increased reinforcement hardness and reduced plastic deformation capability at higher SiC contents. This observation supports a negative

correlation between SiC content and dispersion uniformity [45]. As shown in Table 2, crystallite size decreases with increasing SiC content. This trend is attributed to the combined effects of cold welding of Al particles, followed by their fragmentation induced by the abrasive nature of SiC nanoparticles and localized stress concentrations at the Al/SiC interfaces. The presence of SiC also contributes to crystallite refinement by acting as a barrier to dislocation motion, thereby inhibiting grain growth and promoting structural stability.

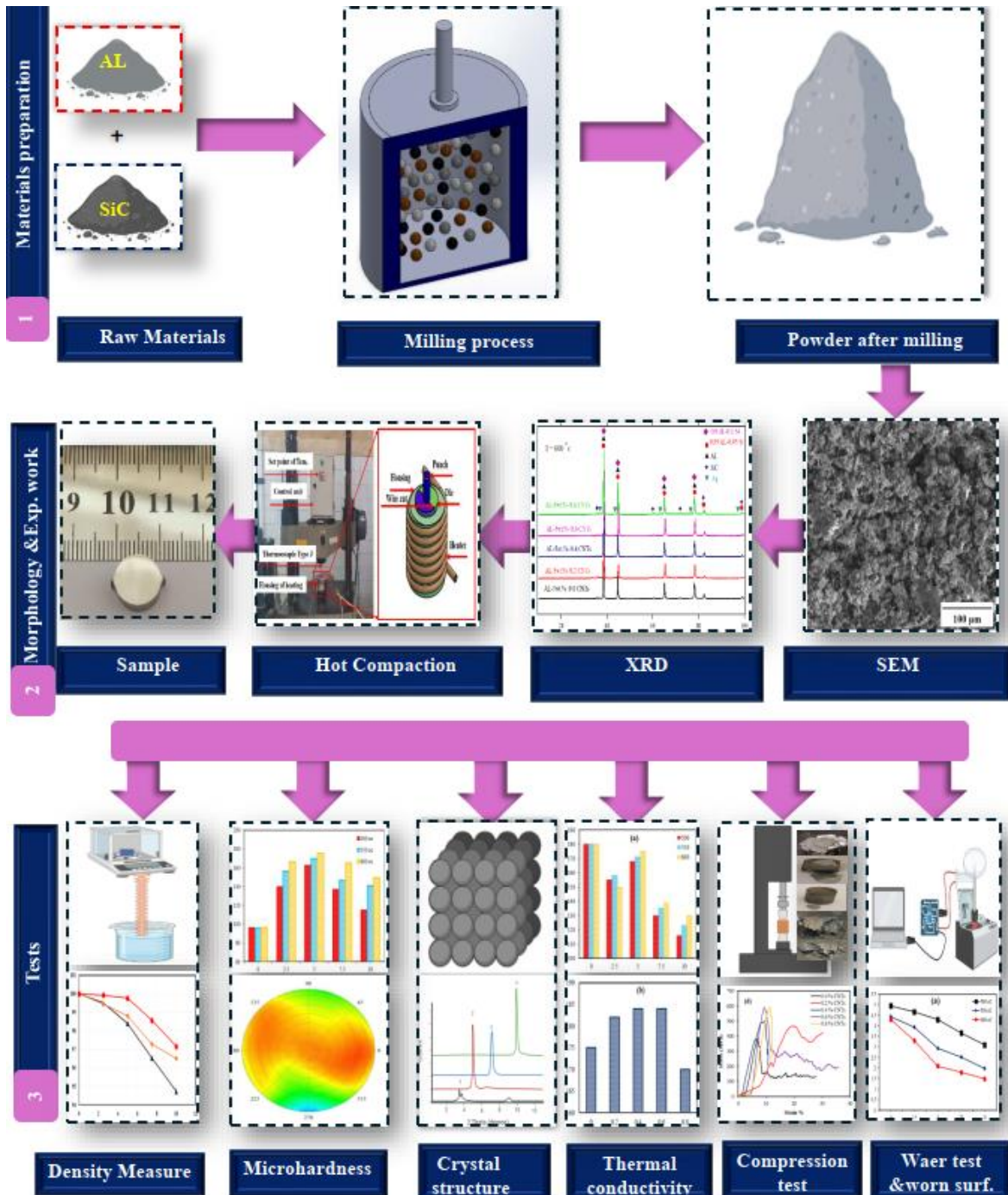


Fig. 5: Schematic image of the different stages for fabricated the Al/SiC nanocomposites by high energy ball milling followed with hot compaction.

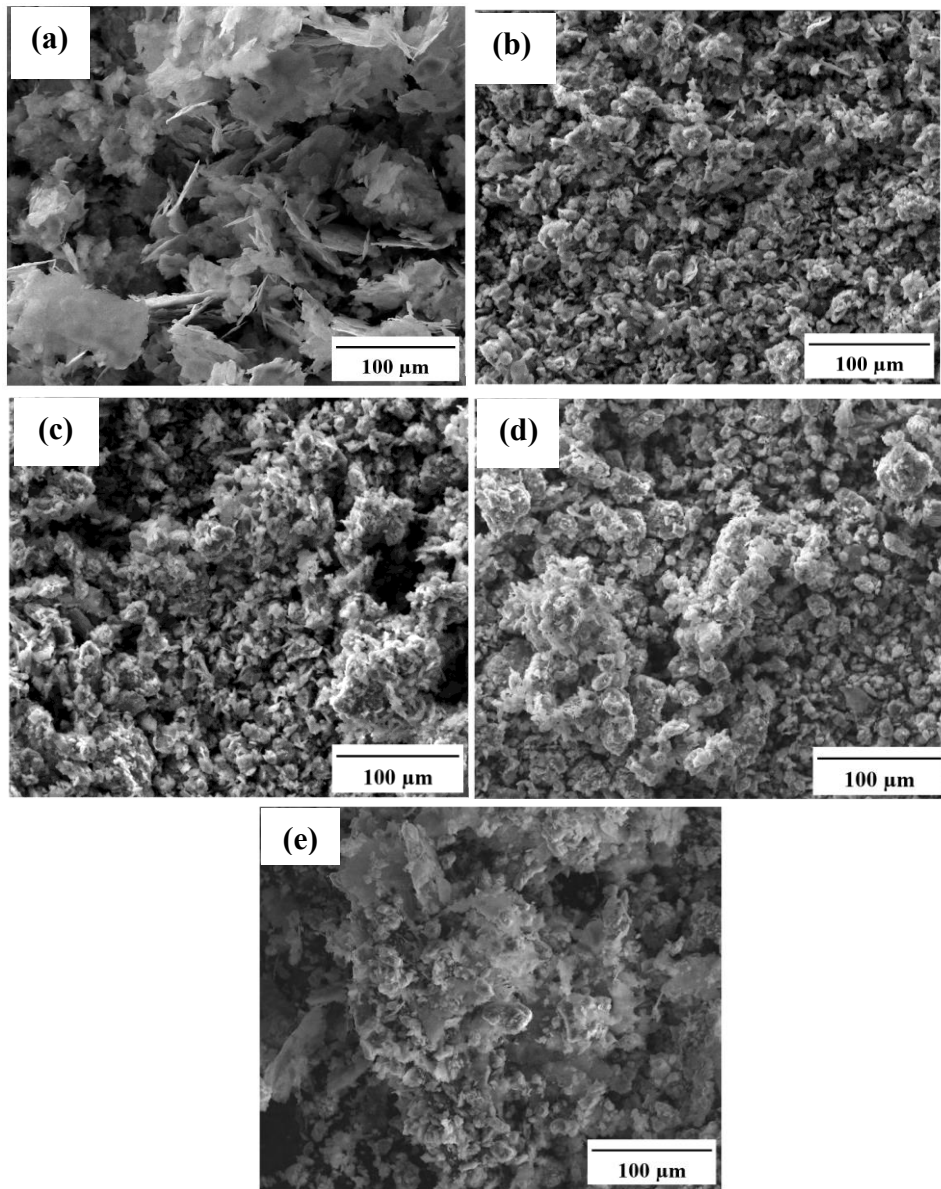


Fig. 6: FE-SEM micrographs of Al/SiC powder (a)0, (b)2.5, (c)5, (d)7.5, and (e)10 wt.% SiC after mixing process.

Fig. 7 presents FE-SEM images of Al/SiC composites with 2.5, 5, 7.5, and 10 wt.% SiC after processing at 600 °C. Fig. 7(a) shows that the 2.5 wt.% sample exhibits a uniform distribution of SiC particles, resulting from homogeneous mixing and good bonding, enhanced by high flowability during hot compaction. However, small micro-voids are observed at particle interfaces due to trapped air, and minor SiC agglomeration is evident [46]. The hot compaction process also influences crystallite size, as 600 °C is close to the recrystallization point of Al, leading to particle growth. Fig. 7(b) illustrates the microstructure of the 5 wt.% SiC composite, where the SiC particles are uniformly dispersed in the Al matrix. This uniform distribution leads to improved particle bonding and fewer micro-voids, with minimal SiC agglomeration [47]. The enhanced bonding is attributed to the higher SiC content and good flowability during compaction. In Fig. 7(c), for the 7.5 wt.% SiC composite, the distribution of SiC particles becomes less uniform, with noticeable agglomeration. This increased agglomeration results from the mechanical alloying process and contributes to more micro-

voids compared to the 2.5 and 5 wt.% SiC samples. The larger grain size during hot compaction, along with air entrapment, exacerbates these issues, which are reflected in a decrease in relative density [48]. Fig. 7(d) shows the microstructure of the 10 wt.% SiC composite, where excessive agglomeration and void formation are evident. These issues become more pronounced by increasing SiC content beyond 7.5 wt.%. Overall, the best improvement in bonding, reduced voids, and minimal agglomeration was observed in the 5 wt.% SiC composite [49].

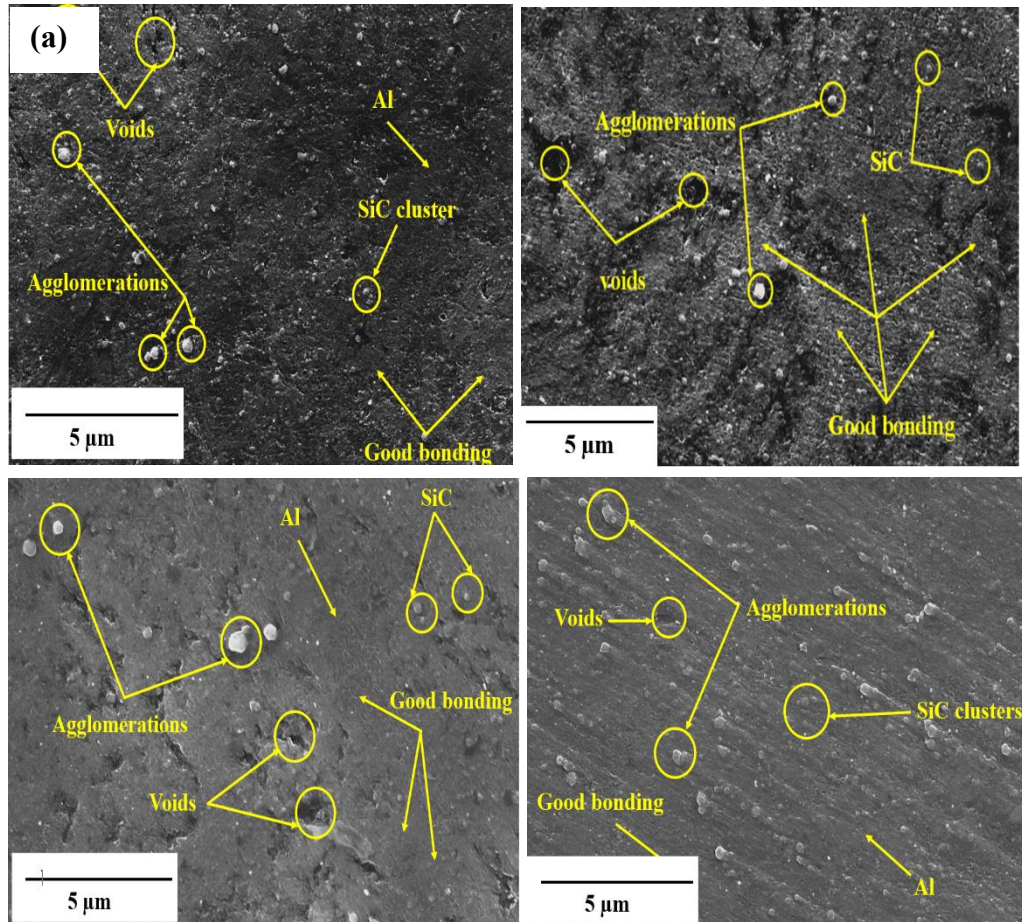


Fig. 7. FE-SEM micrographs of Al/SiC nanocomposites with (a) 2.5, (b) 5, (c) 7.5, and (d) 10 wt.% SiC processed at 600°C.

4.2 Phase and crystalline identification of fabricated samples after hot compaction

The phase constitution of Al/SiC nanocomposites fabricated via hot compaction was evaluated using XRD, as shown in Fig. 8 (a-c). The XRD patterns are influenced by factors such as chemical composition, processing temperature, and SiC reinforcement content. Fig. 8(a) and 8(b) present the diffraction spectra for composites containing 0, 2.5, 5, 7.5, and 10 wt.% SiC, compacted at 550 °C and 600 °C, respectively. At 550 °C, the XRD patterns exhibit lower crystallinity and reduced peak intensities, attributable to increased lattice strain and dislocation density, which promote void formation and particle agglomeration. No evidence of intermetallic phase formation between Al and SiC is observed at this temperature [50]. In contrast, composites sintered at 600 °C show signs of intermetallic compound formation, such as Al-Si phases, likely due to enhanced atomic diffusion facilitated by prior high-energy ball

milling. This interfacial reaction contributes to improved densification and mechanical integrity, particularly in samples containing up to 5 wt.% SiC. However, higher reinforcement levels (7.5 and 10 wt.%) result in excessive particle clustering, heterogeneous dispersion, and defect formation, which suppress further interfacial phase development and compromise microstructural uniformity.

To enhance the quantitative depth of the XRD analysis, full width at half-maximum (FWHM) values were extracted for the dominant (111) Al diffraction peak near $2\theta \approx 38^\circ$. Crystallite sizes were calculated using the Scherrer equation, and lattice strain was estimated using the Williamson–Hall (W-H) method. The analysis revealed that increasing SiC content led to progressive peak broadening and a corresponding decrease in crystallite size, indicative of grain refinement and increased lattice strain. Specifically, the crystallite size was found to decrease from approximately 58.4 nm at 0 wt.% SiC to around 35.2 nm at 10 wt.% SiC, while the lattice strain increased from 1.23×10^{-3} to 2.48×10^{-3} . These findings confirm the role of nano-SiC in suppressing Al grain growth and inducing internal lattice distortion. Among the tested compositions, the 5 wt.% SiC sample exhibited the most favourable combination of refined grain size and moderate strain, correlating well with its enhanced mechanical properties. This integrated XRD assessment reinforces the significant influence of SiC reinforcement on microstructural evolution and performance characteristics in Al-based nanocomposites. XRD analysis revealed no distinct peaks corresponding to Al_4C_3 , indicating that no significant interfacial carbide formation occurred under the applied sintering conditions (up to 600 °C for a short duration). This indicates that the processing parameters were below the threshold required for Al/SiC interfacial reactions involving carbide formation. Furthermore, microscopy investigations confirmed clean and coherent matrix-reinforcement interfaces, with no observable signs of interfacial degradation, thereby validating the thermal and chemical stability of the composite system and eliminating the risk of deteriorative phases such as Al_4C_3 that could impair mechanical and corrosion performance.

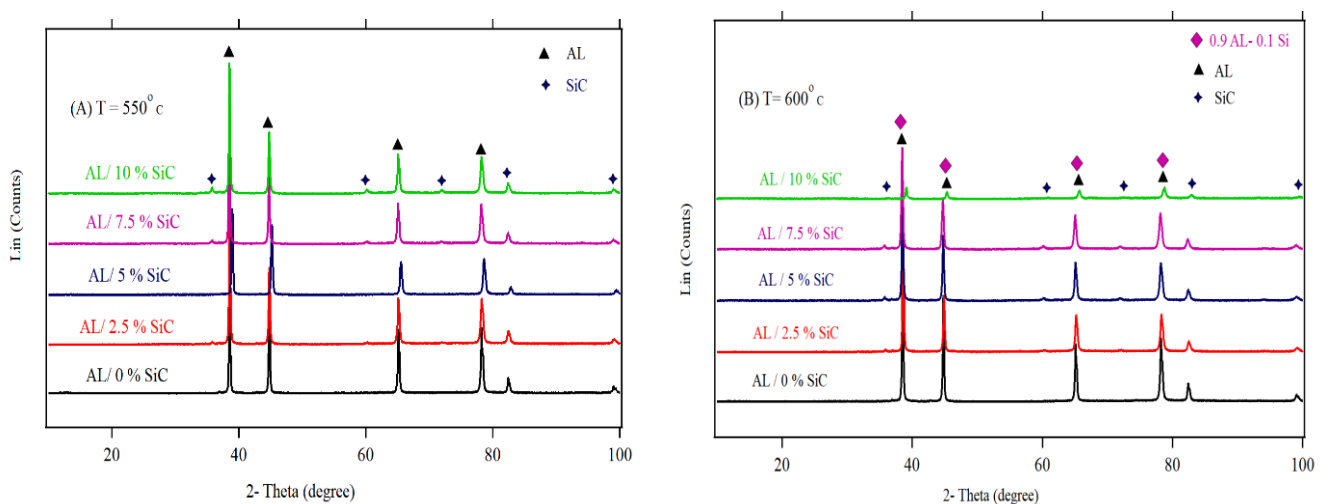


Fig. 8: XRD patterns of Al / SiC (A) 550 and (B) Al / SiC at 600 °C.

Table 2 presents the crystallite sizes of Al/SiC nanocomposites as determined by XRD analysis, highlighting the influence of both SiC content and hot compaction temperature (500 °C, 550 °C, and 600 °C). Increasing the compaction temperature generally promotes grain growth due to recrystallization; however, the presence of SiC particles significantly suppresses this effect. Acting as effective grain boundary pinning agents, SiC reinforcements hinder grain coarsening, facilitating the development of a finer and more stable microstructure. As shown in Table 2, crystallite size decreases progressively with higher SiC content. At 500 °C, for example, the crystallite size is reduced from 138 nm for the unreinforced Al matrix to 90 nm for the 10 wt.% SiC composite. A similar trend is observed at 600 °C, where crystallite size drops from 168 nm to 126 nm as SiC content increases. This grain refinement strongly correlates with enhanced mechanical properties, such as improved hardness and strength, through the Hall-Petch mechanism. The increased grain boundary density impedes dislocation motion, thereby strengthening the composite. However, while mechanical performance benefits from finer grains, thermal conductivity may be compromised due to increased phonon scattering at grain boundaries and defect positions. This introduces a performance trade-off: moderate SiC additions (e.g., 2.5-5 wt.%) yield an optimal balance between strength and thermal conductivity, whereas excessive SiC content (7.5-10 wt.%) leads to excessive refinement and interfacial resistance, ultimately limiting heat transfer. Therefore, precise control over reinforcement content and processing temperature is essential to tailor the microstructure for desired mechanical and thermal performance.

Table 2 Crystallite size (nm) of several contents of Al / SiC at different temperatures.

wt. % SiC	Crystallite size (nm) at different values of temperature		
	500°C	550°C	600°C
0	138	143	168
2.5	123	135	157
5	117	128	148
7.5	112	121	136
10	90	109	126

4.3 SEM and EDX of Al/SiC nanocomposite after hot compaction

Fig. 9 displays SEM micrographs coupled with corresponding EDX spectra for Al/SiC nanocomposites reinforced with 10 wt.% SiC, processed via hot compaction. The SEM images Fig.9 (a-c) represent different scanned regions across the composite surface, as denoted by the colored boxes. These micrographs reveal a relatively uniform surface morphology with fine-scale contrast variations indicative of particle embedding. The EDX spectra obtained from each region consistently shows three major elemental peaks: Al, carbon (C), and silicon (Si). The dominance of the Al peak confirms the prevalence of the aluminum matrix. Meanwhile, the presence of Si and C peaks in all three regions affirms the successful incorporation of SiC reinforcement particles. Notably, the intensity and relative consistency of Si and C signals across the scanned areas suggest a uniform distribution of SiC particles within the Al matrix. This uniform dispersion is a crucial factor for achieving isotropic mechanical and thermal properties, as it ensures homogeneous stress transfer and minimizes

localized stress concentrations. Furthermore, the absence of peaks associated with oxygen or other impurities indicates minimal oxidation and no detectable contamination during the hot compaction process. This confirms effective environmental control and the thermal stability of both the matrix and reinforcement phases during processing. The SEM images support these findings, showing well-distributed, fine bright regions likely corresponding to SiC particles, embedded within the darker Al matrix. The lack of agglomeration and the uniform grey contrast further suggest efficient mixing and compaction. Similar EDX profiles across multiple areas reinforce the conclusion of microstructural homogeneity, which is vital for mechanical reliability and repeatability in composite performance.

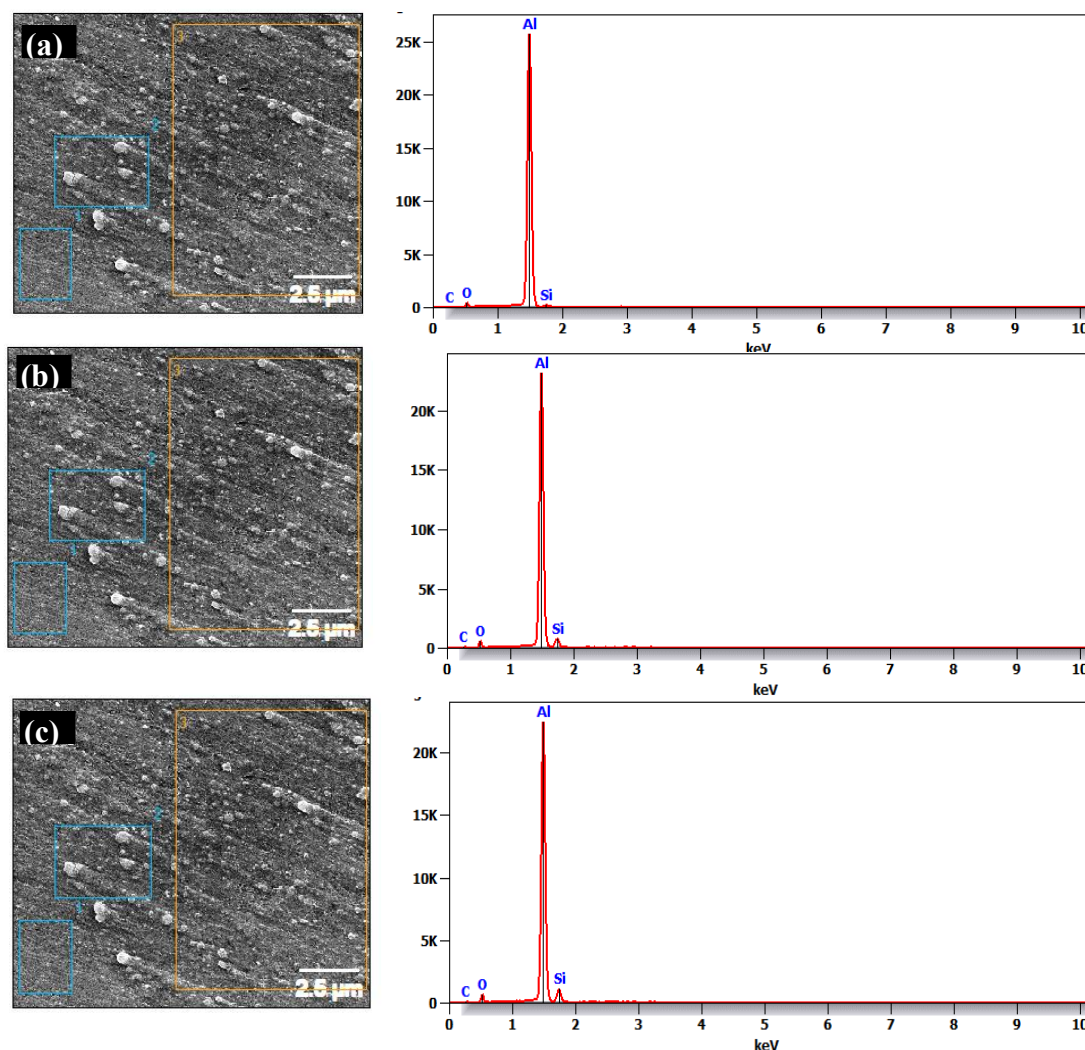


Fig. 9 SEM/EDX Analysis of Al/10 wt.% SiC Nanocomposites

4.4 Physical properties of Al /SiC nanocomposites.

Fig. 10 (a) illustrates the relative density of Al nanocomposites reinforced with varying SiC contents 0, 2.5, 5, 7.5, and 10 wt.% hot compacted at 500, 550, and 600 °C. For unreinforced Al (0 wt.% SiC), the relative density approaches ~100% at all processing temperatures, owing to the high purity and excellent flowability of the Al powder, combined with optimal hot compaction parameters. In contrast, the addition of SiC results in a progressive decrease in relative density across all hot compaction temperatures. For instance, at 600 °C, the relative densities for 2.5, 5, 7.5, and 10 wt.% SiC are observed to be 99.92%, 99.75%, 98.56%, and

97.16%, respectively. Comparable trends are evident at 500 °C and 550 °C [51]. This reduction in relative density with increasing SiC content is primarily attributed to particle agglomeration and micropore formation during hot compaction, as corroborated by the FE-SEM micrographs in Fig.7. At higher SiC concentrations, agglomeration induces heterogeneous regions within the matrix, disrupting uniform distribution and leading to increased porosity and diminished densification. The influence of compaction temperature is also significant. Elevated temperatures promote higher relative density due to enhanced plastic deformation of Al grains and improved material flow. As the temperature increases from 500 °C to 550 °C, a modest increase in density is noted for all compositions. For example, the 10 wt.% SiC sample shows an increase in relative density from 94.73% at 500 °C to 96.5% at 550 °C. At 600 °C, the densification becomes more pronounced, particularly for the 5 wt.% SiC composite, which reaches 99.75%, approaching full theoretical density. This enhancement is attributed to the proximity of the processing temperature to the recrystallization range of Al, facilitating plastic flow and pore elimination. These findings agree with the morphological observations presented in Fig. 7 and the crystallite size data in Table 2.

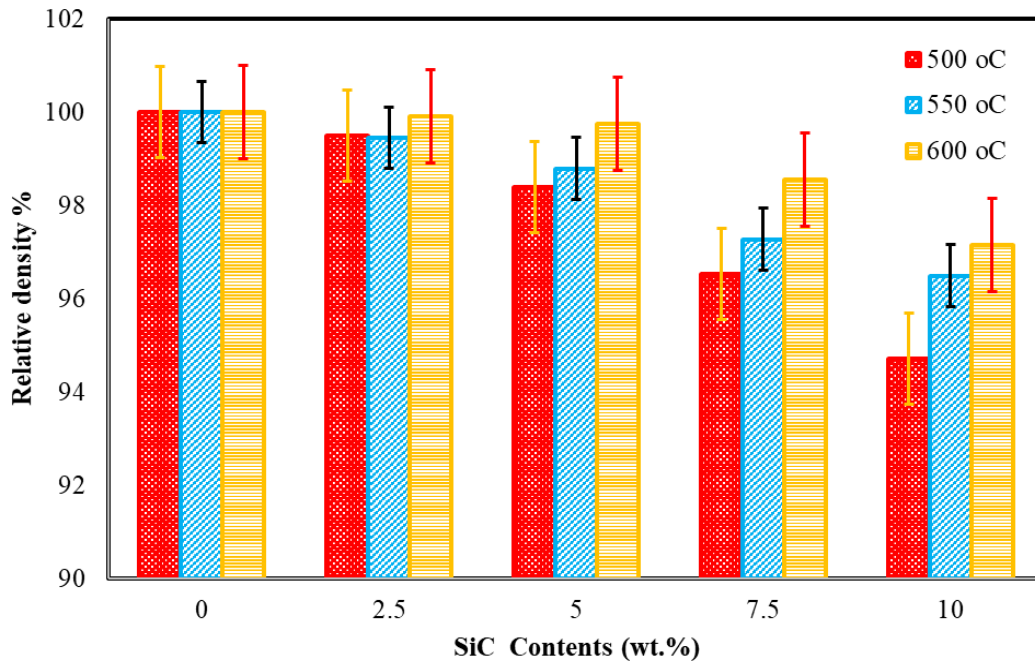


Fig. 10: Relative density of Al / SiC (a) 500, 550 and 600 °C nanocomposite at 600°C.

Al is widely recognized for its high thermal conductivity ($\sim 200 \text{ W.m}^{-1}\cdot\text{K}^{-1}$), making it a favourable matrix for thermally conductive composites. Silicon carbide (SiC), a ceramic with a thermal conductivity of approximately $120 \text{ W.m}^{-1}\cdot\text{K}^{-1}$. Enhances thermal performance when incorporated into an Al matrix by introducing secondary pathways for heat transfer. The actual conductivity of SiC, however, varies based on its purity and microstructural characteristics. Fig. 11 illustrates the thermal conductivity of Al/SiC nanocomposites containing 0, 2.5, 5, 7.5, and 10 wt.% SiC, fabricated via hot compaction at 500, 550, and 600 °C. For the unreinforced Al sample 0 wt.% SiC, thermal conductivity remains near $120 \text{ W.m}^{-1}\cdot\text{K}^{-1}$ across all temperatures, wing to the high purity, superior flowability, and near-full

densification of the Al matrix [52]. As the SiC content increases, a general decline in thermal conductivity is observed, primarily attributed to particle agglomeration and the formation of micro-voids, which reduce relative density and disrupt heat conduction pathways as shown in Fig. 11.

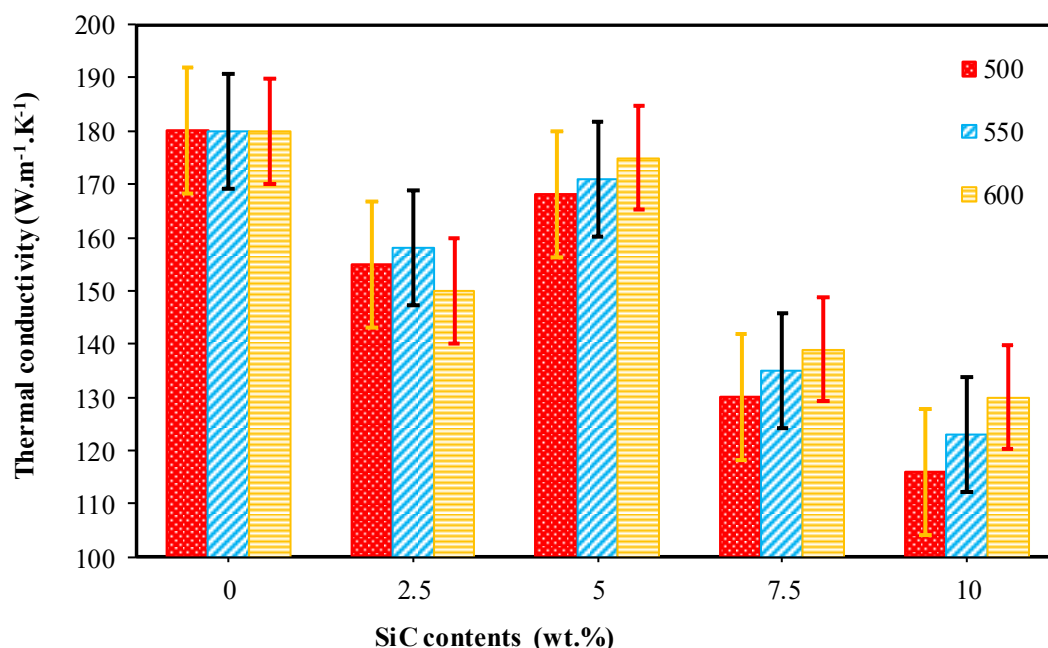


Fig. 11: Thermal conductivity of Al / SiC (a) 500, 550 and 600 °C nanocomposite.

4.5 Mechanical and tribological characteristics of Al/ SiC nanocomposites:

Fig. 12(a) presents the microhardness of Al/SiC nanocomposites with 0, 2.5, 5, 7.5, and 10 wt.% SiC, compacted at temperatures of 500, 550, and 600 °C. The microhardness of the composites increased at all compaction temperatures with the addition of SiC up to 5 wt.%; however, a decrease in microhardness was observed at higher SiC contents of 7.5 and 10 wt.%. The addition of SiC up to 5 wt.% improved microhardness due to the effective dispersion of SiC particles, which restrict dislocation motion within the Al matrix and enhance its load-bearing capacity. At 5 wt.%, an optimal level of particle dispersion was achieved, enhancing the interaction between SiC particles and the Al matrix, thus improving the load transfer mechanism. At higher compaction temperatures 600 °C, the microhardness increased significantly, from 96.55 HV for pure Al to 175.26 HV for Al-5 wt.% SiC, representing an 81.5% increase. However, at SiC contents of 7.5 and 10 wt.%, the microhardness decreased despite the higher SiC content. This reduction was attributed to the agglomeration of SiC particles and the formation of micro voids, which led to poor particle distribution and reduced relative density as shown in Fig. 10. These structural defects hindered the load transfer mechanism, thus reducing the hardness that had been improved with lower SiC content. As noted by [53] and Ye et al. [22], a reduction in particle size, increased surface area, and enhanced strain energy at the particle-matrix interface contribute to strengthening the composite, improving microhardness up to 5 wt.% SiC. Beyond this concentration, SiC agglomeration and decreased density limit the mechanical advantages. Thus, the optimal mechanical properties are achieved when SiC content is at or below 5 wt.%, where particle

dispersion and matrix interaction are maximized, preventing agglomeration. Furthermore, the effect of compaction temperature on microhardness was also observed, with microhardness increasing as temperature rose, which is in line with the relative density results shown in Fig. 10.

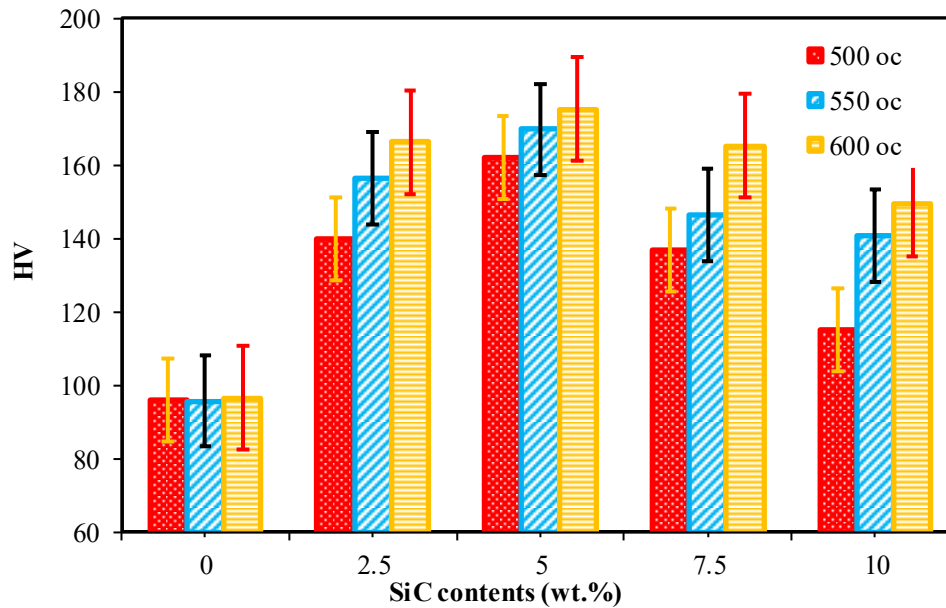


Fig. 12: Hardness values of Al / SiC nanocomposites.

The microhardness mapping was conducted using a circular mapping technique with consistent radial and angular spacing to ensure uniform coverage and reliable comparative analysis across the sample surface. Each measurement point maintained a fixed radial distance from the center, and angular intervals were precisely maintained to ensure reproducibility of orientation-based comparisons. As shown in Fig. 13, the microhardness distribution across the Al/SiC composite reveals distinct spatial variations. Higher hardness values were recorded near the outer periphery of the sample, particularly where the powder compact interfaces with the mold wall. This is likely due to localized stress concentrations and better particle compaction during processing. Similarly, the upper surface exhibits elevated hardness compared to the inner core, possibly due to differential heat dissipation and compaction dynamics during hot pressing. The angular distribution shows a non-uniform pattern: between 0° and 45° , an increase in hardness is observed, which may result from enhanced interfacial bonding and grain refinement in these regions. Between 45° and 90° , a decline in hardness values is noted, potentially due to reduced effective load transfer or particle agglomeration, which can create localized soft spots. From 135° to 225° , hardness increased again, suggesting favorable particle orientation and stress distribution. However, a decline from 225° to 315° indicates possible microstructural inconsistencies or stress-induced softening.

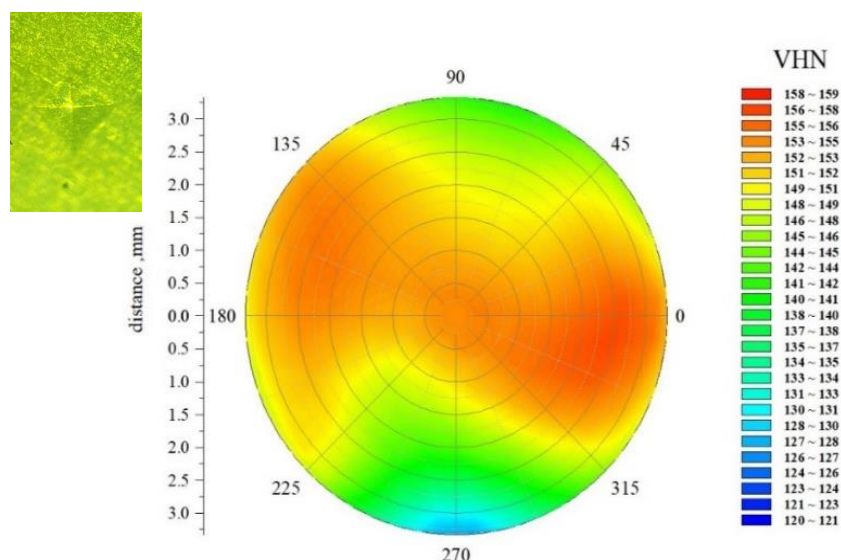


Fig. 13: Microhardness distribution of Al / SiC nanocomposite.

Fig. 14 shows the stress-strain curves of Al/SiC nanocomposites. The effect of SiC content on the compressive strength of Al/SiC nanocomposites indicates that increasing SiC content leads to a rise in compressive strength up to 5 wt.% of SiC, which consistently exhibits superior compressive strength at all temperatures compared to other SiC concentrations. The enhanced performance of the 5 wt.% SiC composite is mainly attributed to reduced void formation, decreased particle agglomeration, improved grain bonding, and higher relative density, all of which contribute to the improved compressive strength. The enhancement is primarily attributed to the uniform distribution of SiC particles within the aluminum matrix, which effectively hinders dislocation motion and contributes to load transfer. Additionally, the increased interfacial bonding and densification at the optimal compaction temperature (600 °C) resulted in fewer internal defects and improved structural integrity, further strengthening the composite under compressive loads. Furthermore, the fracturing patterns of these samples, as shown in Fig. 15, confirm the structural improvements. Composites containing 2.5, 7.5, and 10 wt.% SiC demonstrated greater compressive strength than those with 0 wt.% SiC but showed reduced strength compared to the 5 wt.% SiC composite. This behavior can be linked to the recrystallization of the aluminum matrix, which enhances ductility while still maintaining adequate compressive strength.

Fig. 14 (a-c) illustrates the stress-strain behavior of Al/SiC composites hot-compacted at three different temperatures: (a) 500 °C, (b) 550 °C, and (c) 600 °C. The corresponding peak compressive strengths are 523.7 MPa, 523.23 MPa, and 631.8 MPa, respectively. The results clearly demonstrate that increasing the hot compaction temperature to 600 °C leads to improved compressive strength, particularly for the composite containing 5 wt.% SiC, which shows the highest strength at this temperature (Fig. 14c). This enhancement is attributed to improved material flowability, enhanced particle diffusion, and near-full densification under high compaction pressure, which collectively result in better interfacial bonding and reduced porosity.

Furthermore, detailed analysis of the stress-strain curves reveals significant changes in plastic deformation behavior with temperature. At higher temperatures, the plastic deformation region becomes more extended for composites with lower SiC content (0 wt.% and 2.5 wt.%), suggesting increased ductility, likely due to dynamic recrystallization of the Al matrix. In contrast, composites with higher SiC content (7.5 wt.% and 10 wt.%) exhibit reduced strain-to-fracture and a less pronounced plastic region. This is attributed to particle agglomeration, which acts as stress concentrators, reducing ductility despite the elevated temperature. Additionally, the slope of the initial linear region of the stress-strain curves allow for estimation of the elastic modulus, which tends to increase with moderate SiC additions (2.5-5 wt.%) but becomes inconsistent allowed loadings due to microstructural defects. The fracture strain also varies significantly, highlighting the brittle-to-ductile transition across different SiC contents and processing temperatures. Therefore, the inclusion of full stress-strain analysis provides a more comprehensive understanding of the mechanical behavior beyond peak strength, especially in the plastic regime where the interplay between matrix softening and particle strengthening becomes critical.

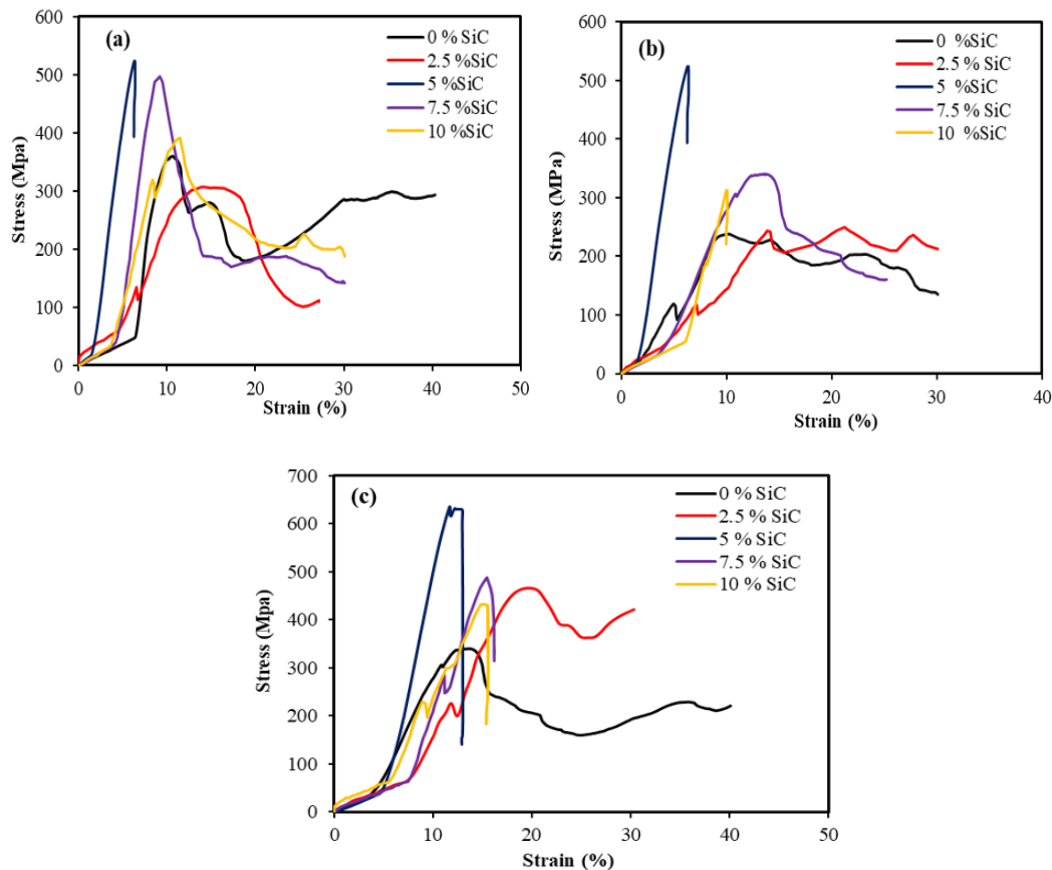


Fig. 14: Stress-strain curves of Al/SiC nanocomposites processed at (a) 500 °C, (b) 550 °C, and (c) 600 °C.

Fig. 14 illustrates the fracture behaviour of Al/SiC composites with varying SiC contents subjected to different hot compaction temperatures. At 500 °C, the samples exhibited reduced relative densities, leading to increased cracking and fragmentation during the compression

test. This reduction in density is likely due to insufficient particle bonding and limited material flow at lower compaction temperatures, which adversely impacted the microstructure. At 550 °C, greater damage was observed in the pure Al and the 2.5, 7.5, and 10 wt.% SiC composites, whereas the 5 wt.% SiC sample remained more structurally intact. This improved performance is attributed to better interfacial bonding and enhanced structural integrity at the optimal reinforcement level of 5 wt.% SiC, which effectively limited the extent of fracture during compaction [54]. At the elevated hot compaction temperature of 600 °C, the pure Al sample showed more extensive damage compared to the 5 wt.% SiC composite. The superior performance of the 5 wt.% SiC composite is likely due to the presence of SiC particles providing reinforcement and improved resistance to crack propagation under high-temperature compression. In summary, compaction at 600 °C resulted in more structurally sound samples across all compositions, with the 5 wt.% SiC composites demonstrating the highest resistance to fracture, highlighting the synergistic effect of optimal reinforcement and elevated processing temperature.

At Constant pressure = 900 Mpa






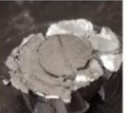






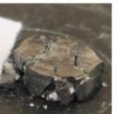


Wt. % & R.den. Temp. ° c	0% SiC	Relative Density %	2.5% SiC	Relative Density %	5 % SiC	Relative Density %	7.5 % SiC	Relative Density %	10% SiC	Relative Density %
500		99.89		98.22		98.03		96.53		94.73
550		100.00		100.00		100.00		97.28		96.50
600		100.00		100.00		100.00		98.56		97.16

Fig. 15: Fracture morphologies of Al–SiC nanocomposites compacted at 500, 550, and 600 °C for each sample.

4.6 Wear rate and coefficient of friction measurements of Al / SiC nanocomposites:

Fig. 16 illustrates the effect of SiC content and hot compaction temperature on the wear resistance of Al/SiC nanocomposites. The incorporation of SiC significantly enhances wear resistance, with the most notable improvements observed up to 5 wt.% SiC. Beyond this concentration, the rate of improvement diminishes, likely due to micropore formation during the hot compaction process. Additionally, increasing the compaction temperature from 500 °C to 600 °C substantially reduces the wear rate. This enhancement is attributed to microstructural refinement, including better SiC particle dispersion and increased composite hardness. Elevated compaction temperatures contribute to reduced wear debris by promoting

a more uniform distribution of reinforcement particles, which minimizes vacancy formation and suppresses dislocation motion. These factors collectively improve the hardness and wear resistance of the composite [55]. Overall, both the SiC content and the compaction temperature play critical roles in optimizing the structural integrity and tribological performance of Al/SiC nanocomposites.

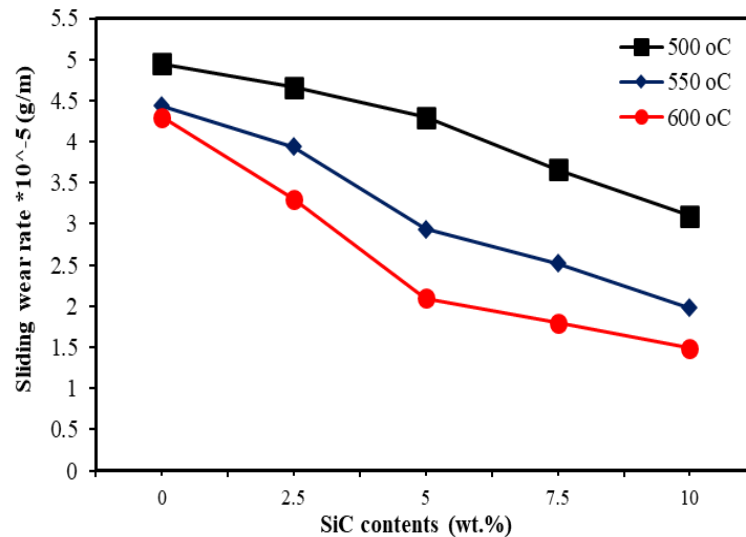


Fig. 16: Wear rate of Al / SiC nanocomposites at 500, 550, and 600°C.

Fig. 17 presents the average coefficient of friction (COF) for Al/SiC nanocomposites hot compacted at 500, 550, and 600 °C. The compaction temperature plays a significant role in influencing the tribological properties of the nanocomposites, particularly at higher SiC concentrations. The results demonstrate that both the SiC content and the compaction temperature are critical factors affecting the COF of Al/SiC nanocomposites. Elevated compaction temperatures enhance interfacial bonding between Al and SiC particles, thereby improving the composite's structural integrity and tribological performance [56]. This strengthened bonding contributes to increased wear resistance and a reduction in friction coefficients during testing. Additionally, increasing the SiC content further modifies the COF behavior by reinforcing the matrix and altering the contact mechanics at the sliding interface. Frictional heating at the sliding interface can influence COF by locally raising surface temperatures, potentially softening the Al matrix or inducing thermal stresses at the Al–SiC interface. These effects may alter wear mechanisms and COF behaviour during testing. While temperature was not directly measured, all tests were conducted under identical conditions to ensure consistency. Future studies should incorporate in-situ temperature monitoring to better assess thermal effects.

This section examines the worn surfaces of Al/SiC nanocomposites subjected to wear testing to evaluate the influence of compaction temperature and SiC content on tribological performance. To isolate the effect of temperature on wear behaviour, samples containing an optimal 5 wt.% SiC were fabricated at 500 °C, 550 °C, and 600 °C, as presented in Fig. 18. Among these, the sample hot compacted at 600 °C demonstrated superior wear resistance, attributed to enhanced densification, improved interfacial bonding, and reduced material

degradation under abrasive conditions. This improvement is supported by the reduced wear rate Fig. 16 and lower COF values Fig. 17, indicating enhanced surface stability and resistance to abrasion. Elevated compaction temperatures likely modify surface and subsurface characteristics, resulting in improved mechanical integrity during sliding contact. To further assess the role of reinforcement content, worn surface morphologies were analyzed using SEM for samples hot compacted at 600 °C with varying SiC contents 0, 5, and 10 wt.%, as shown in Fig. 19.

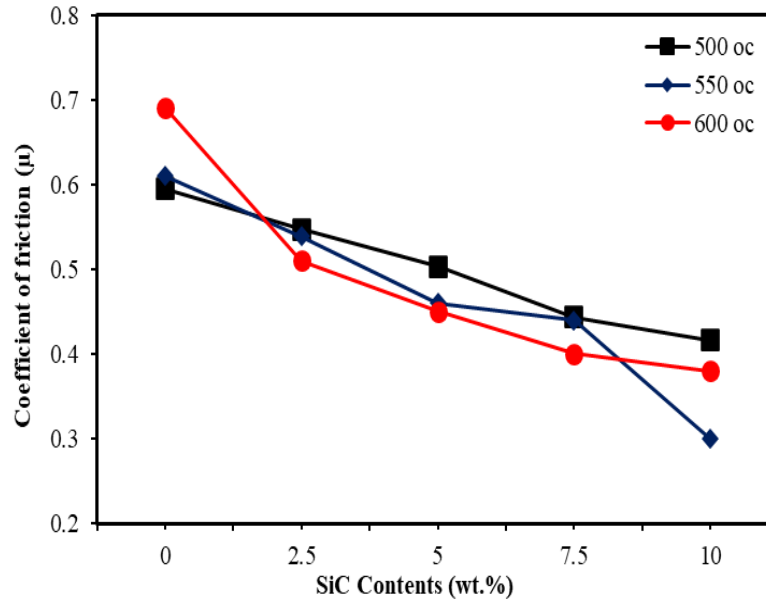


Fig. 17: Coefficient of friction of Al / SiC nanocomposites at 500, 550, and 600°C.

The sample with 5 wt.% SiC exhibited homogenous ploughing marks, uniform abrasive direction, and well-dispersed reinforcement particles Fig. 19, reflecting a balanced microstructure with optimal load transfer and wear resistance. In contrast, samples with 0 wt.% and 10 wt.% SiC showed surface defects such as friction-induced layers, delamination, non-uniform particle distribution, and micro-cracking typical indicators of surface degradation. These features suggest increased susceptibility to wear, likely due to insufficient reinforcement or agglomeration effects at higher SiC content. Frictional layers indicate thermal and mechanical stress accumulation during wear, which compromises surface performance and may initiate subsurface damage.

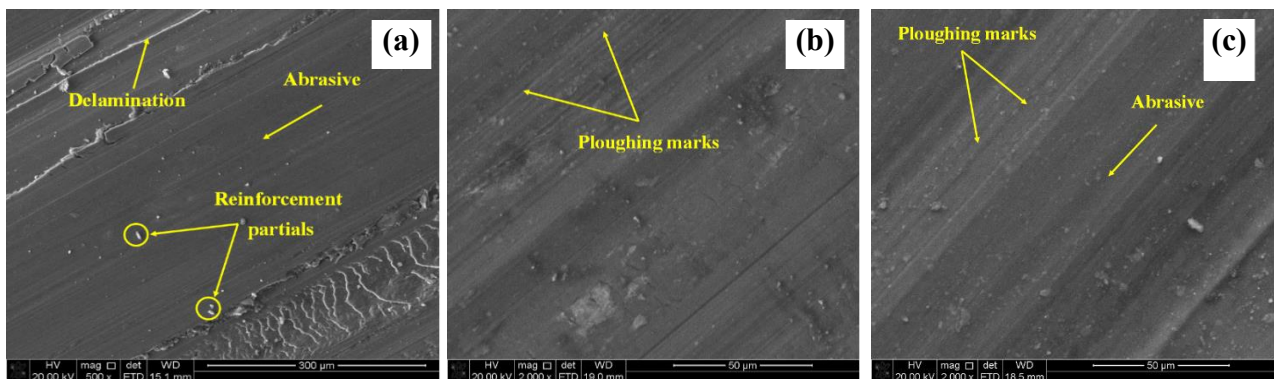


Fig.18 Worn surface for Al / 5 wt.% SiC composites (a) 500, (b) 550 and (c) 600°C.

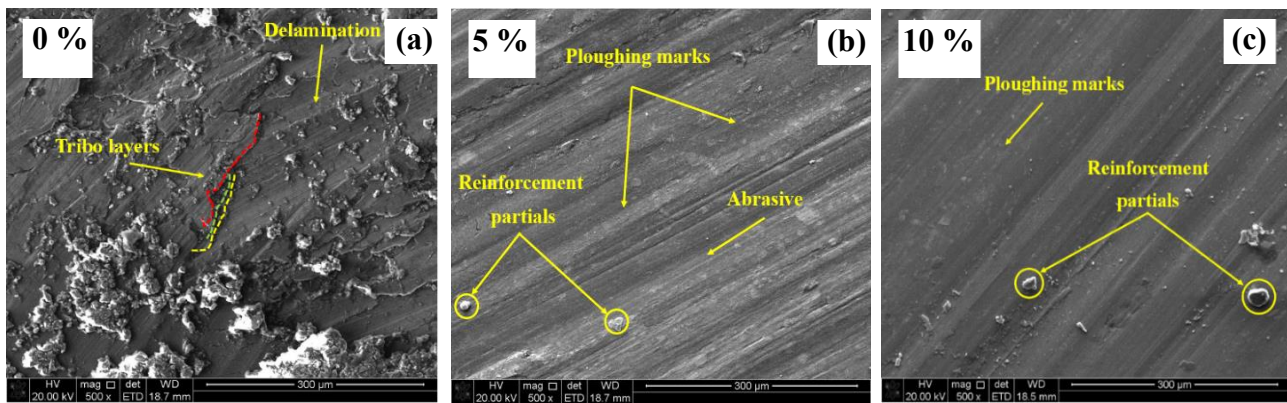


Fig.19 Worn surface for Al / SiC (a) 0 %, (b) 5%, (c)10% SiC composites at 600°C.

5. Conclusions

The conclusions and novel insights derived from this study are outlined as follows:

- Homogeneous distribution of reinforcements and microstructural refinement: The addition of 5 wt.% SiC through mechanical alloying and hot compaction resulted in a uniform dispersion of reinforcement particles within the aluminum matrix, enhancing the quality of interfacial bonding.
- Influence of Compaction Temperature on Densification: Samples compacted at 600 °C exhibited better structural integrity and increased relative density compared to those processed at 500 °C and 550 °C. These improvements are attributed to enhanced particle bonding and material hot compaction at higher temperatures.
- The addition of 5 wt.% SiC to the Al matrix significantly enhanced its mechanical properties, resulting in a peak hardness of 179 HV and improved compressive strength compared to samples compacted at lower temperatures (500 °C and 550 °C).
- Under a 15 N load, the 5 wt.% SiC composites showed the lowest wear rate (2.7×10^{-5} g/min.), confirming it as the optimal content for enhancing wear resistance and minimizing material loss.
- The Al nanocomposite exhibited surface damage such as ploughing marks and delamination, indicating low wear resistance under the test conditions.
- In comparison, the 5 wt.% SiC nanocomposites displayed a smoother worn surface with minimal defects, highlighting the reinforcing benefits of SiC particles.

References

- [1] Hafizpour, H.R., Simchi, A. and Parvizi, S., 2010. Analysis of the compaction behavior of Al-SiC nanocomposites using linear and non-linear compaction equations. *Advanced Powder Technology*, 21(3), pp.273-278.
- [2] Ye, T., Xu, Y. and Ren, J., 2019. Effects of SiC particle size on mechanical properties of SiC particle reinforced aluminum metal matrix composite. *Materials Science and Engineering: A*, 753, pp.146-155.
- [3] Tan, Z., Chen, Z., Fan, G., Ji, G., Zhang, J., Xu, R., Shan, A., Li, Z. and Zhang, D., 2016. Effect of particle size on the thermal and mechanical properties of aluminum composites reinforced with SiC and diamond. *Materials & Design*, 90, pp.845-851.

- [4] Shojaeefard, M.H., Akbari, M., Khalkhali, A., & Asadi, P. 2018. Effect of tool pin profile on distribution of reinforcement particles during friction stir processing of B₄C/aluminum composites. *Proceedings of the Institution of Mechanical Engineers, Part L: Journal of Materials: Design and Applications*, **232**(8), 637–651.
- [5] Akbari, M., Shojaeefard, M.H., Asadi, P. and Khalkhali, A., 2019. Wear and mechanical properties of surface hybrid metal matrix composites on Al–Si aluminum alloys fabricated by friction stir processing. *Proceedings of the Institution of Mechanical Engineers, Part L: Journal of Materials: Design and Applications*, **233**(5), pp.790-799.
- [6] Wang, Z., Song, M., Sun, C. and He, Y., 2011. Effects of particle size and distribution on the mechanical properties of SiC reinforced Al–Cu alloy composites. *Materials Science and Engineering: A*, **528**(3), pp.1131-1137.
- [7] Wang, H., Zhang, R., Hu, X., Wang, C.A. and Huang, Y., 2008. Characterization of a powder metallurgy SiC/Cu–Al composite. *Journal of materials processing technology*, **197**(1-3), pp.43-48.
- [8] Fathy, A., Sadoun, A. and Abdelhameed, M., 2014. Effect of matrix/reinforcement particle size ratio (PSR) on the mechanical properties of extruded Al–SiC composites. *The International Journal of Advanced Manufacturing Technology*, **73**, pp.1049-1056.
- [9] Narayanasamy, R., Ramesh, T. and Prabhakar, M., 2009. Effect of particle size of SiC in aluminium matrix on workability and strain hardening behaviour of P/M composite. *Materials Science and Engineering: A*, **504**(1-2), pp.13-23.
- [10] Tan, Z., Chen, Z., Fan, G., Ji, G., Zhang, J., Xu, R., Shan, A., Li, Z. and Zhang, D., 2016. Effect of particle size on the thermal and mechanical properties of aluminum composites reinforced with SiC and diamond. *Materials & Design*, **90**, pp.845-851.
- [11] Narayanasamy, R., Ramesh, T. and Prabhakar, M., 2009. Effect of particle size of SiC in aluminium matrix on workability and strain hardening behaviour of P/M composite. *Materials Science and Engineering: A*, **504**(1-2), pp.13-23.
- [12] Yu, H.O.N.G., Wang, W.J., Liu, J.Q., Tang, W.M. and Wu, Y.C., 2019. Effect of porosity and interface structures on thermal and mechanical properties of SiCp/6061Al composites with high volume fraction of SiC. *Transactions of Nonferrous Metals Society of China*, **29**(5), pp.941-949.
- [13] Penther, D., Ghasemi, A., Riedel, R., Fleck, C. and Kamrani, S., 2018. Effect of SiC nanoparticles on manufacturing process, microstructure and hardness of Mg–SiC nanocomposites produced by mechanical milling and hot extrusion. *Materials Science and Engineering: A*, **738**, pp.264-272.
- [14] Khadem, S.A., Nategh, S. and Yoozbashizadeh, H., 2011. Structural and morphological evaluation of Al–5 vol.% SiC nanocomposite powder produced by mechanical milling. *Journal of Alloys and Compounds*, **509**(5), pp.2221-2226.
- [15] Hassan, A., El-Hamid, A., Wagih, A. and Fathy, A., 2014. Effect of mechanical milling on the morphology and structural evaluation of Al–Al₂O₃ nanocomposite powders. *International Journal of Engineering*, **27**(4), pp.625-632.
- [16] Yildirim, M., Özyürek, D. and Gürü, M., 2016. Investigation of microstructure and wear behaviors of al matrix composites reinforced by carbon nanotube. *Fullerenes, Nanotubes and Carbon Nanostructures*, **24**(7), pp.467-473.
- [17] Simões, S., Viana, F., Reis, M.A. and Vieira, M.F., 2014. Improved dispersion of carbon nanotubes in aluminum nanocomposites. *Composite structures*, **108**, pp.992-1000.
- [18] Javadi, A., Mirdamadi, S., Faghihisani, M., Shakhesi, S. and Soltani, R., 2013. Well-dispersion of multi-walled carbon nanotubes in aluminum matrix composites by controlling the mixing process. *Fullerenes, Nanotubes and Carbon Nanostructures*, **21**(5), pp.436-447.

- [19] Mhaske, M.S. and Shirsat, U.M., 2021. An investigation of mechanical properties of aluminum based silicon carbide (AlSiC) metal matrix composite by different manufacturing methods. *Materials Today: Proceedings*, 44, pp.376-382.
- [20] Zulfia, A., Atkinson, H.V., Jones, H. and King, S., 1999. Effect of hot isostatic pressing on cast A357 aluminum alloy with and without SiC particle reinforcement. *Journal of materials science*, 34, pp.4305-4310.
- [21] Yu, H., Wang, W., Liu, J., Tang, W., Wu, Y., 2019. Effect of porosity and interface structures on thermal and mechanical properties of SiCp/6061Al composites with high volume fraction of SiC. *Trans. Nonferrous Met. Soc. China* 29(5), 941–949.
- [22] Ye, T., Xu, Y. and Ren, J., 2019. Effects of SiC particle size on mechanical properties of SiC particle reinforced aluminum metal matrix composite. *Materials Science and Engineering: A*, 753, pp.146-155.
- [23] El-Kady, O. and Fathy, A., 2014. Effect of SiC particle size on the physical and mechanical properties of extruded Al matrix nanocomposites. *Materials & Design (1980-2015)*, 54, pp.348-353.
- [24] Jiang, W., Zhu, J., Li, G., Guan, F., Yu, Y. and Fan, Z., 2021. Enhanced mechanical properties of 6082 aluminum alloy via SiC addition combined with squeeze casting. *Journal of Materials Science & Technology*, 88, pp.119-131.
- [25] Iqbal, A.K.M., Lim, M.J. and Nuruzzaman, D.M., 2017, December. Effect of compaction load and sintering temperature on the mechanical properties of the Al/SiC nano-composite materials. In *AIP Conference Proceedings* Vol. 1901, No. 1. AIP Publishing.
- [26] Abu-Oqail, A.M.I., Elmashad, A.M., El-Sheikh, M.N., Mohamed, M.M., El-Sayed, H.A., 2024. Mechanical and tribological performance of Al–xSiC composites produced by powder metallurgy technique for throttle valves applications. *J. Egypt. Soc. Tribol.* 21(3), 55–73.
- [27] Canakci, A., & Varol, T. (2014). Microstructure and properties of AA7075/Al–SiC composites fabricated using powder metallurgy and hot pressing. *Powder Technology*, 268, 72–79.
- [28] Ünlü, B. S. 2008. Investigation of tribological and mechanical properties of Al₂O₃–SiC reinforced Al composites manufactured by casting or P/M method. *Materials & Design*, 29(10), 2002–2008.
- [29] Akbari, M., Shojaeefard, M.H., Asadi, P. and Khalkhali, A., 2019. Wear and mechanical properties of surface hybrid metal matrix composites on Al–Si aluminum alloys fabricated by friction stir processing. *Proceedings of the Institution of Mechanical Engineers, Part L: Journal of Materials: Design and Applications*, 233(5), pp.790-799.
- [30] Singh, J., 2016. Fabrication characteristics and tribological behavior of Al/SiC/Gr hybrid aluminum matrix composites: A review. *Friction*, 4, pp.191-207.
- [31] Karamış, M. B., Sari, F. N., & Erturun, V. 2012. Friction and wear behaviors of reciprocatingly extruded Al–SiC composite. *Journal of Materials Processing Technology*, 212(12), 2578–2585.
- [32] Ahmadian, H., Zhou, T., Guo, W., Yu, Q., Sadoun, A.M., Fathy, A. and Wagih, A., 2024. A novel strategy for activation technique for 6H-SiC substrates in electroless Ni-P plating processes. *Results in Engineering*, 24, p.103126.
- [33] Alsoruji, G.S., Sadoun, A.M., Abd Elaziz, M., Al-Betar, M.A., Abdallah, A.W. and Fathy, A., 2023. On the prediction of the mechanical properties of ultrafine grain Al-TiO₂ nanocomposites using a modified long-short term memory model with beluga whale optimizer. *Journal of Materials Research and Technology*, 23, pp.4075-4088.
- [34] Najjar, I.M.R., Sadoun, A.M., Ibrahim, A., Ahmadian, H. and Fathy, A., 2023. A modified artificial neural network to predict the tribological properties of Al-SiC nanocomposites

- fabricated by accumulative roll bonding process. *Journal of Composite Materials*, 57(21), pp.3433-3445.
- [35] Bor, A., Jargalsaikhan, B., Uranchimeg, K., Lee, J. and Choi, H., 2021. Particle morphology control of metal powder with various experimental conditions using ball milling. *Powder technology*, 394, pp.181-190.
- [36] Atkins, Edward. "Elements of X-ray Diffraction." 1978: 572.
- [37] Little, J.E., Yuan, X. and Jones, M.I., 2012. Characterisation of voids in fibre reinforced composite materials. *Ndt & E International*, 46, pp.122-127.
- [38] Mousa, M.M., Mohammed, M.M., El-Kady, O.A. and Mohamed, H.S., 2024. Microstructure, hardness, electrical, and thermal conductivity of SZCN solder reinforced with TiO₂ and ZrO₂ nanoparticles fabricated by powder metallurgy method. *Journal of Materials Science: Materials in Electronics*, 35(17), p.1133.
- [39] Dak, G. and Pandey, C., 2021. Experimental investigation on microstructure, mechanical properties, and residual stresses of dissimilar welded joint of martensitic P92 and AISI 304L austenitic stainless steel. *International Journal of Pressure Vessels and Piping*, 194, p.104536.
- [40] Odabas, D., 2018. Effects of load and speed on wear rate of abrasive wear for 2014 Al alloy. In *IOP conference series: materials science and engineering* Vol. 295, No. 1, p. 012008. IOP Publishing.
- [41] Suryanarayana, C., & Al-Aqeeli, N. 2013. Mechanically alloyed nanocomposites. *Progress in Materials Science*, 58(4), 383-502.
- [42] Benjamin, J. S. 1970. Dispersion strengthened superalloys by mechanical alloying. *Metallurgical Transactions*, 1(10), 2943-2951.
- [43] Ye, T., Xu, Y. and Ren, J., 2019. Effects of SiC particle size on mechanical properties of SiC particle reinforced aluminum metal matrix composite. *Materials Science and Engineering: A*, 753, pp.146-155.
- [44] Fogagnolo, J. B., et al. 2003. Effect of mechanical alloying on the morphology, microstructure, and properties of Al–SiC composites. *Materials Science and Engineering: A*, 355(1-2), 50-54.
- [45] Chen, J.P., Gu, L. and He, G.J., 2020. A review on conventional and nonconventional machining of SiC particle-reinforced aluminum matrix composites. *Advances in Manufacturing*, 8(3), pp.279-315.
- [46] Li, Q., Yuan, S., Li, Z., Gao, X. and Chen, B., 2023. Mechanical response and microstructure evolution of SiC particle-reinforced Al-MMCs under ultrasonic loading. *Composites Part A: Applied Science and Manufacturing*, 173, p.107657.
- [47] Zhang, X., Li, S., Pan, D., Pan, B. and Kondoh, K., 2018. Microstructure and synergistic-strengthening efficiency of CNTs-SiCp dual-nano reinforcements in aluminum matrix composites. *Composites Part A: Applied Science and Manufacturing*, 105, pp.87-96.
- [48] Asgharzadeh, H. and McQueen, H.J., 2015. Grain growth and stabilisation of nanostructured aluminum at high temperatures. *Materials Science and Technology*, 31(9), pp.1016-1034.
- [49] Gurmaita, P.K., Pongen, R. and Gurmaita, S.K., 2024. A7075 alloy reinforced metal matrix composites fabricated through stir casting route: A review. *International Journal of Cast Metals Research*, 37(3), pp.208-255.
- [50] Wang, Y. and Monetta, T., 2023. Systematic study of preparation technology, microstructure characteristics and mechanical behaviors for SiC particle-reinforced metal matrix composites. *Journal of Materials Research and Technology*, 25, pp.7470-7497.
- [51] Momohjimoh, I., Hussein, M.A. and Al-Aqeeli, N., 2019. Recent advances in the processing and properties of alumina–CNT/SiC nanocomposites. *Nanomaterials*, 9(1), p.86.

- [52] Rajpoot, S., Ha, J.H. and Kim, Y.W., 2021. Effects of initial particle size on mechanical, thermal, and electrical properties of porous SiC ceramics. *Ceramics International*, 47(6), pp.8668-8676.
- [53] Melaibari, A., Fathy, A., Mansouri, M. and Eltaher, M.A., 2019. Experimental and numerical investigation on strengthening mechanisms of nanostructured Al-SiC composites. *Journal of Alloys and Compounds*, 774, pp.1123-1132.
- [54] Froes, F. H., Suryanarayana, C., & Frazier, W. E. 1997. "Advanced powder metallurgy of light metal matrix composites." *JOM (Journal of the Minerals, Metals & Materials Society)*, 49(5), 15-19.
- [55] Huo, S., Xie, L., Xiang, J., Pang, S., Hu, F. and Umer, U., 2018. Atomic-level study on mechanical properties and strengthening mechanisms of Al/SiC nano-composites. *Applied Physics A*, 124, pp.1-12.
- [56] Tan, C., Ma, W., Deng, C., Zhang, D. and Zhou, K., 2023. Additive manufacturing SiC reinforced maraging steel: Parameter optimisation, microstructure and properties. *Advanced Powder Materials*, 2(1), p.100076.